Solid Freeform Fabrication 2021: Proceedings of the 32nd Annual International
Solid Freeform Fabrication Symposium – An Additive Manufacturing Conference
Reviewed Paper

INVESTIGATING THE EFFECT OF HEAT TRANSFER ON THE HOMOGENITY IN MICROSTRUCTURE AND PROPERTIES OF INCONEL 718 ALLOY FABRICATED BY LASER POWDER BED FUSION TECHNIQUE

B. Farhang*, B.B. Ravichander*, A. Ganesh-Ram*, S. Ramachandra*, M. Hanumantha*, W. Hall*, A. Dinh*, A. Amerinatanzi*†, N. Shayesteh Moghaddam*

*Mechanical & Aerospace Engineering, University of Texas at Arlington, Arlington, TX.
†Materials Science and Engineering, University of Texas at Arlington, Arlington, TX.

Abstract

Laser Powder Bed Fusion (LPBF) of metallic components is associated with microstructure and inhomogeneity of properties in the fabricated components. In a recent work by the authors, a novel technique of considering a border surrounding the main part during the LPBF fabrication is proposed to address the issue of inconsistency in microstructure across the cross section of LPBF-fabricated parts. This study, on the other hand, aims to investigate the effect of such border on the microstructure homogeneity along the build direction of LPBF-fabricated parts. For this purpose, a cubic sample surrounded by a cubic border was fabricated to control the rate of heat transfer and then improve the microstructure across the cross section. Also, a sample with identical dimensions and the same process parameters was printed without border as a reference to be compared. To investigate the variation of the properties along the build direction, microstructure and hardness results were compared between areas near and away the substrate for both samples. For the area away from the substrate, in both samples, a deeper pool, less surface porosity, and higher Vickers hardness was observed compared to the area near the substrate. It was found out that, regardless of the focused area, the sample fabricated with border possesses deeper pools, higher level of density as well as higher hardness value. However, in term of homogeneity along the build direction, no significant improvement was observed for the sample fabricated with the cubic border.

Keywords: Laser powder bed fusion, Inconel 718, Microstructure, Vickers Hardness, Homogeneity.

1. Introduction

Nickel-based superalloys are widely utilized in industrial applications such as energy production, aerospace, and aeronautical applications [1-3]. Some of their applications include turbine blades, engine components, combustors, and nuclear power plant parts because of their resistance to corrosion and strength [4, 5]. A particularly well-studied nickel-based alloy, Inconel 718 (IN718), is used in a wide range of industrial sectors. Well-suited mechanical properties such as high creep, fatigue, and corrosion resistance at elevated temperatures have created implementations of this alloy in forceful conditions at temperatures over 700 ◦C [1, 6, 7]. To achieve near-ideal mechanical properties, IN718 is fabricated in the form of casting, forging, wrought, and powder metallurgy [8, 9]. However, along with developments in the manufacturing, the demand for the production of complex parts with higher dimensional accuracy and better mechanical properties at high temperatures have increased. As a solution, manufacturing near-net custom parts can be

performed using the Additive Manufacturing (AM) technique. Compared to many conventional manufacturing techniques, AM is considered a less costly method since it does not require additional industrial manufacturing components such as casting dies and molds [1, 10, 11]. Considering both industrial and developmental aspects, manufacturing IN718 components using AM has drawn considerable attention over the last decade [12-17]. The Laser Powder Bed Fusion (LPBF), as a commonly used method in AM [4], provides high level of complexity and meanwhile high precision in fabrication of metal components. Through induction of pools arising from melted powders, LPBF is able to fabricate full-dense metallic components (close to 99.7% [4]). In this method, the metallic powder is selectively melted using a laser source, which is tracked based on part specifications from imported design data. The molten powders merge making a combined hardened layer. This process repeats on each layer until the fabrication is complete. Although it has been revealed that LPBF is capable of production of IN718 components with high densification level and acceptable mechanical properties[18-21], improvements in the mechanical properties of LPBF fabricated IN718 parts are still being researched [8].

LPBF fabricated IN718 contains a valuable, distinct multi-scale microstructure [8] which can be altered along with its texture to suit the needed specifications and properties of the part. The majority of studies on the microstructure and texture of LPBF processed IN718 focused on adjusting the processing parameters such as laser power, scanning speed, layer thickness of powder, and hatch space [1, 8, 9, 13, 17, 22-25]. These parameters affect the volume energy density (VED) and thereby impacting the microstructure, texture and finally properties of the as-fabricated parts. Moussaoui *et al*. [26] demonstrated for LPBF fabricated IN718 specimens, in case of microstructure, increase in VED results in lengthened dendrites orienting along the build direction. They also found that the level of porosity is inversely related to VED. Nadammal *et al*.[27] examined the influence of hatch space on the microstructure and texture of LPBF processed IN718. It was concluded that increase in hatch space caused the texture intensity to decrease by a ratio of 10:2. A study performed by Lu *et al*. [24], examined different island scanning strategies for the fabrication of IN718 parts. They showed that components created by using island scanning strategies 5×5 and 7×7 mm^2 have the highest density while 2×2 mm^2 showed critical cracks. In another study on scan speed and density of IN718, researchers concluded that an extensive range of scanning speed (from 100 to 1600 mm/s) can be utilized to produce parts successfully with the highest density level (99.7%) being achieved at the laser scanning speed of 800 mm/s [28]. Popovich *et al*. [29] showed that the layer thickness is directly proportional to cell size of LPBF fabricated microstructure of IN718 with higher formation chances of columnar grain structure. In another study, the effect of process parameters on Vickers hardness of LPBF processed IN718 was investigated [30]. It was concluded that the hatch spacing has the most effect on the hardness of the samples, with a reverse relationship being found between these parameters. Kumar *et al*. [31] studied he effect of laser power and scan speed on the porosity level of LPBF fabricated IN718. A linear increase in the porosity level was observed when the scanning speed increased. By contrast, increasing the laser power led to a significant reduction in the porosity level.

The understanding of the physics involved in the LPBF process is as important as controlling the effect of the laser process parameters to tailor the microstructure of the part for its final application. As a high temperature process, the heat transfer occurring during LPBF is an important physical parameter that can be controlled. A phase filed model study of IN718 revealed that the temperature gradient is a key factor in dendrite growth, with temperature gradient being directly

proportional to the speed of dendrite growth [32]. However, not only the melting step, but also the solidification and cooling process should be considered in LPBF technique. Zhang *et al*. [33], developed a physical model to simulate the thermofluidic field of molten pools formed during the LPBF process of IN718. It was shown that convective heat transfer influences the shape of the melt pool more than conduction heat transfer, since the contribution of convection in heat dissipation is higher by an order. They also found that width of the melt pool is a function of only convection while the depth is a function of both conduction and convection. However, there is no comprehensive study investigating the variation of heat transfer modes on the IN718 microstructure produced by LPBF as most research focused on post-processing.

In a recent study performed by authors, the effect of convective heat transfer on the microstructure and properties of LPBF fabricated IN718 samples was examined. For this purpose, cubic borders were used to surround the cubic samples in order to limit the convective heat transfer during the fabrication process. It was found out that using the surrounding border leads to better mechanical properties and higher densification level. In this study, authors aimed to examine the effect of convective heat transfer through a cubic border on the homogeneity of the microstructure, densification levels, and microhardness along the height of LPBF-fabricated IN718 samples.

2. Material and Methods

2.1. Materials and Fabrication

The material used in this study was gas atomized IN718 powder supplied by EOS North America (Pflugerville, TX, USA). The composition of the powder can be found here [34]. Two different part designations were selected to fabricate in the current study (see table 1). A cubic sample surrounded by a cubic border and another cubic sample without a border was printed for reference. Based on the previous study performed by the authors, 0.5 mm gap value resulted in the best properties for the sample and therefore in this study the gap between border and the sample was fixed to be 0.5 mm. Figure 1 shows the schematic of the sample surrounded by the border and the fabricated parts used in this study.

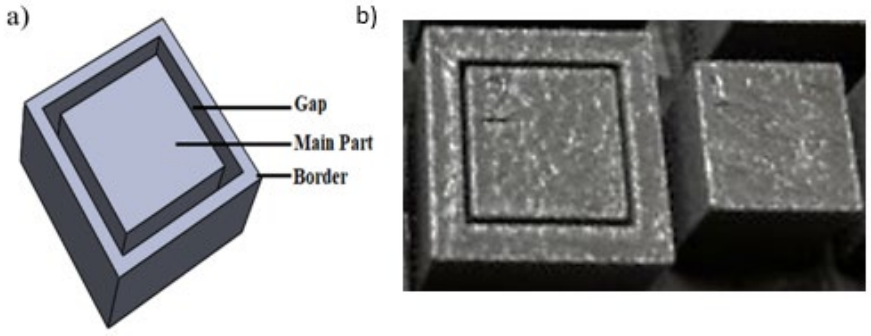

Figure 1. a) schematic of sample with border, b) sample fabricated with border on the left (Gap 0.5 sample) and the sample fabricated without border on the right (reference sample)

Table 1. Geometry and dimensions of the fabricated samples

Sample No./Name	Type of Geometry	Sample Dimensions (mm)	Border Dimensions (mm)	Gap Between Sample and Shell (mm)
Gap 0.5	Cubic	9×9×6 (w×l×h)	6×2 (H×t)	0.5
Reference Sample	Cubic	9×9×6 (w×l×h)	-	-

1: w, l and h are width, lengths and height of the main sample respectively.
2: H and t are height and thickness of the border respectively.

Both the specimens were printed using an EOSINT® M290 400 W Yb:YAG fiber laser and same process parameters (285 W laser power, 110 µm hatching distance, 40 µm layer thickness, 100 µm laser beam diameter, and 960 mm/s scanning speed). The platform was preheated to 80 °C and held at this temperature to reduce the thermal gradient between fabricated parts and the platform. The laser scanning strategy consisted of strip tracks and a hatch angle of 67° in each consecutive layer.

2.2. Experiment Method

A Hitachi S-3000N Variable Pressure Scanning Electron Microscopy (SEM) was used to reveal the microstructure. For sample preparation, prior to mounting, the sample was ultrasonically cleaned, rinsed, and dried with compress air to remove any oil or debris from sectioning or handling. Then, the LPBF fabricated sample was mounted on epoxy resin and hardeners. Grinding and polishing of sample were performed by E-prep 4™ with power head in individual force mode. Grinding was conducted with a series of silicon carbide (SiC) abrasive discs (320 to 1200 Grit size). After each grinding step, the sample surface was inspected using metallographic microscope XJP-H100 (Amscope, Irvine, CA) to ensure the scratch pattern was uniform. Removal of deformation caused by grinding was accomplished using 1 µm diamond suspension on DiaMat polishing cloth with GreenLube lubricant. Final polishing was performed with 0.04 µm colloidal silica suspension on a Chem-pol polishing cloth. To remove debris and abrasive particulates after each grinding and polishing step, the platen was wiped, washed with water, and spin-dried. The sample and fixture were cleaned with micro-organic soap, rinsed with isopropyl alcohol, and then dried using compressed air. The sample was etched by Kalling's 2 Reagent (cupric chloride, hydrochloric acid, and ethanol) [35] before microstructural analysis. The Vickers hardness of samples was measured by LECO LM 300 AT Micro Hardness Tester under 1000 g loads which was applied for 10 seconds. A total of 5 indentations were done to report the average hardness at each selected area.

3. Results and Discussion

3.1. Microstructure Analysis

3.1.1. Melt pools

The melt pools of the reference sample and the Gap 0.5 sample were observed from the SEM images generated at the areas near the substrate (close to the cubic border for the Gap 0.5 sample) as seen in figure 2. As can be observed in figure 1a, shallower pools were formed in the reference sample compared to the sample fabricated with a border (figure 1b). Using ImageJ software [36], a dimensional analysis was performed to extract the depth of the melt pools. The melt-pool analysis was performed according to the NASA MSFC-SPEC-3717 Standard [37] and the ratio of melt-pool depth (d_p) over layer thickness (t_L) was extracted (see figure 1b). Different images were analyzed,

and the average value is reported in table 2. According to the dimensional analysis, around 12 percentage increase in the depth of the pools was noticed for the Gap 0.5 sample. One can attribute this observation to the different heat transfer conditions that underwent in the samples during the fabrication process. For the Gap 0.5 sample which is surrounded by a border, the lateral heat transfer is limited due to the gap and border acting as a barrier. By contrast, for the reference sample, the heat can be dissipated in both lateral and vertical direction (parallel to the build direction) without any limitation. This leads to the different heat transfer conditions between samples., In this case, the amount of heat transferring along the build direction is more for Gap 0.5 sample compared to reference sample. This facilitates the thermal gradient along the build direction for Gap 0.5 sample and therefore molten material can penetrate to greater depths. This, in turn, facilitates overlapping of the melt pools and formation of deeper pools. This observation has been reported in the literature where Mostafa *et al.*[4] and Jia and Gu [13] attributed the formation of deeper pools to the laser track overlapping and steep thermal gradient.

In terms of structure of the pools, more cohesive boundaries can be seen for the Gap 0.5 sample compared to the reference sample. This difference in structure is rooted to different heat transfer conditions discussed above. In response to the overlapping of pools, formation of new boundaries bring about different structure and stronger bonding between neighbouring pools. It is revealed that with increase in the penetartion of molten material into deeper layers, the probability of pools getting overlapped is higher, particularly in the heat affected zones (HAZ) [38, 39]. This phenamenon occurred in the Gap 0.5 sample due to the higher thermal gradient compared to the reference sample. Consequently, new pool boundaries with stronger structures were formed in the sample surrounded by the border.

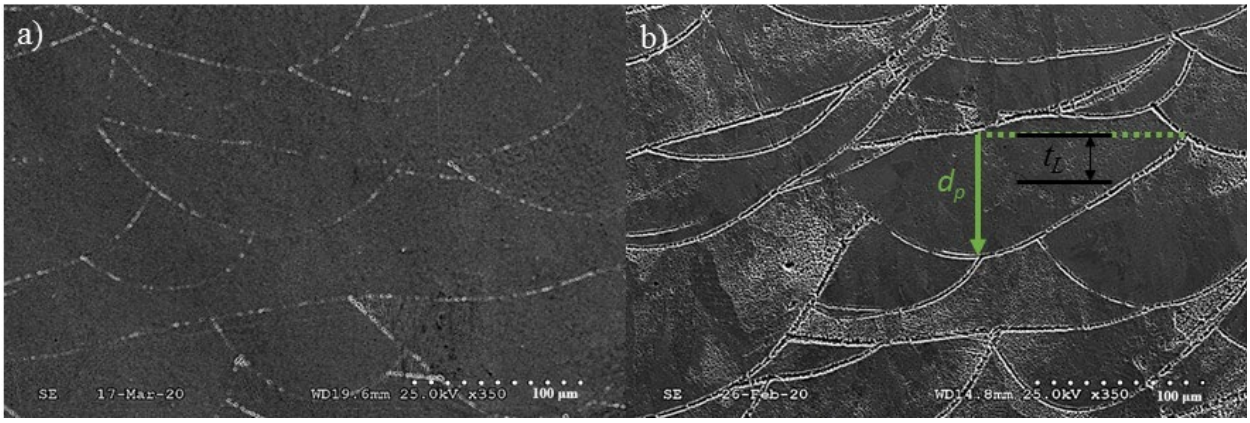

Figure 2. SEM micrographs of melt pools extracted from areas near the substrate for a) reference sample, b) Gap 0.5 sample. Deeper pools with stronger melt pool boundaries were found for Gap 0.5 sample compared to the reference sample. The depth of a melt pool (d_p) was depicted in the figure as a comparison with a layer thickness (t_L).

Figure 3 compares the melt pools for the areas away from the substrate (far from the cubic border for the Gap 0.5 sample). Similar to the results oberved for the area near the substrate, deeper

pools can be seen for the Gap 0.5 sample (figure 3b). As discussed before, the different heat transfer conditions could be attributed to this observation. However, based on the dimensional analysis, the average depth of the pools are higher compared to the ones reported for the region near the substrate. Also, the effect of border on the dimension of pools is more visible for this region as the difference between the depth of pools increased by around 14 percent. It can be infered that the border design considered for the fabrication of Gap 0.5 sample, has more effect on the microstructure for the areas away from the substrate. This outcome is consistent with the observations made by authors in the previous study [40], where different microstructure and better properties were found for the areas away from the substrate. Generally, this difference is rooted to different thermal gradient at different areas of the sample. As the areas near the susbtrate is close to the build plate with significantly lower temperature, the thermal gradient is considerably high which results in extremely fast cooling rate. This prevents formation of deeper pools due to the less time available for heat to prenetrate across layers. On the other hand, for the areas away from the substrate, the conduction occurs between layers with relatively high temperatures. This moderates the thermal gradient to allow the molten material to penetrate into deeper layers. When the border is considered, the direction of heat transfer is guided toward the build direction with conductive heat transfer playing a greater role. This brings about higher thermal gradient along the building direction to some extent to avoid heat dissipation through convection. This mechanism by which conductive heat transfer dominating the convective heat transfer faciliates penetration of molten material into deeper layers, while the cooling rate is not too fast as we can see for the areas near the substrate. That is why although border can affect the thermal gradient and particularly heat transfer mode, it cannot completely moderate the sharp thermal gradient that exists between the layers near the substrate. Therefore, with the sample surrounded by a border (Gap 0.5 sample), a variation in microstrcuture can be observed through the presence of deeper pools that were formed in areas away from the substrate. Also, a better bonding between pools can be observed for the Gap 0.5 sample which corroborates it.

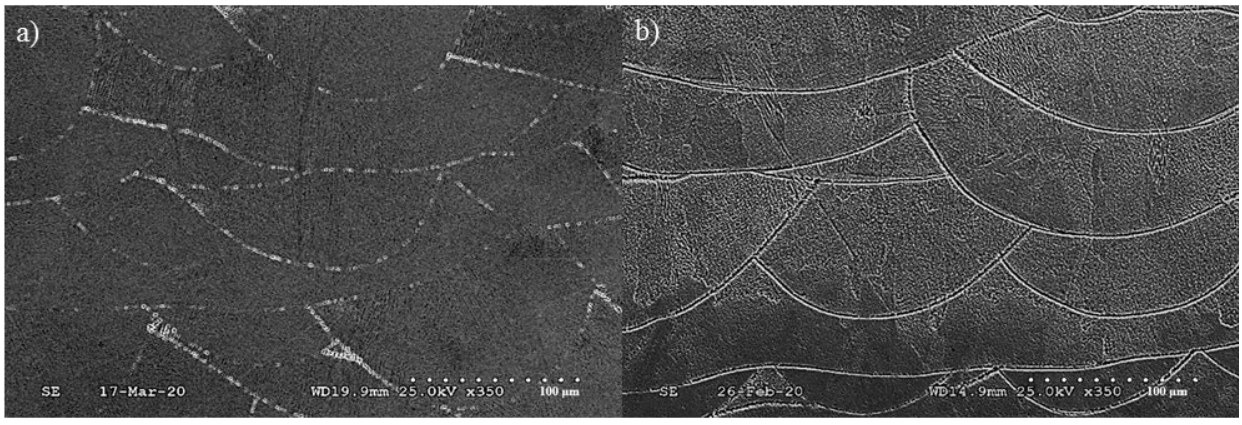

Figure 3. SEM micrographs of melt pools extracted from areas away from the substrate for a) reference sample, b) gap 0.5 sample. While the depth of the pools was higher for the Gap 0.5 sample versus the reference sample, deeper pools were observed for both samples for this area compared to the regions away from the substrate.

Table 2. Dimensional analysis of melt pools perforemd by *ImageJ* software

Sample Name		Reference sample	Gap 0.5
Average Melt Pool Depth over layer thickness	Near the Substrate	2.42	2.72
	Away from the Substrate	2.74	3.07

3.1.2. Defects

Figure 4 demonstrates the surface porosity of samples at the region near the substrate (close to the cubic border for the Gap 0.5 sample), with surface pores being shown using white arrows. Higher number of pores with larger areas can be observed for the reference sample (figure 4a) compared to the Gap 0.5 sample (figure 4b). Using the analysis performed by *ImageJ* software, the level of porosity was extracted for the samples. According to the results, a relatively higher level of surface porosity was found for the reference sample (0.115%) compared to the Gap 0.5 sample (0.089%). The defect size analysis was also performed using the same software. The distribution of the porosities was plotted in terms of defect size for both samples. As can be seen in figure 5, the proportion of larger pores (bigger than 1μm) is considerably higher for the references sample relative to the Gap 0.5 sample. This can again be attributed to the different heat transfer condition provided by the border. It has been revealed that formation of pores in LPBF process is related to the molten metal accumulation due of the high levels of dynamic viscosity [13]. In this case there is a converse relationship between the probability of formation of pores and the flowability of the molten fluid. The sufficiently higher thermal gradient in the building direction facilitated by the border, provides better condition for the molten metal to flow smoothly without any hindrance. This results in the reduction of porosity and presence of finer pores in Gap 0.5 sample, compared to the reference sample as it experiences more convection from lateral direction which acts as a barrier for a smoother flow of molten material.

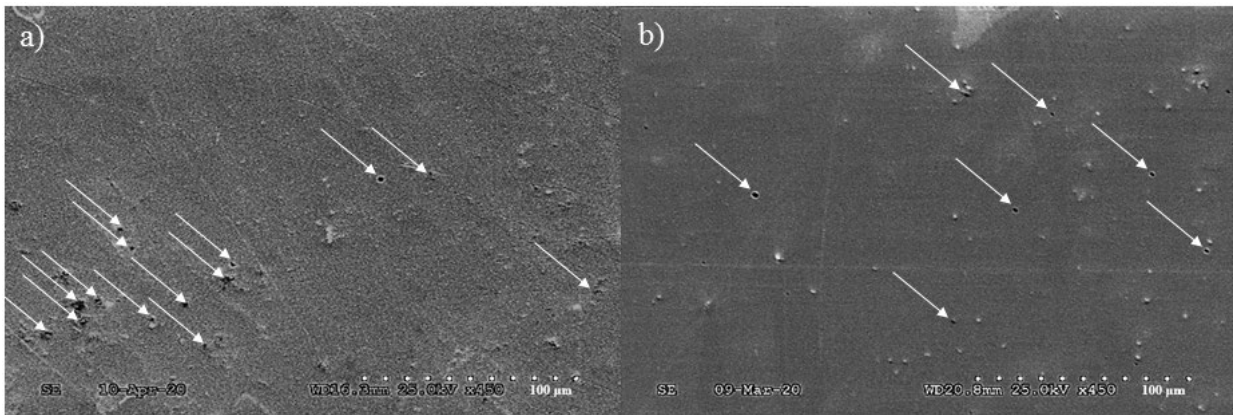

Figure 4. SEM micrographs showing surface porosities formed in areas near the substrate for a) reference sample, b) gap 0.5 sample. Higher number of porous areas were found for the reference sample versus Gap 0.5 sample.

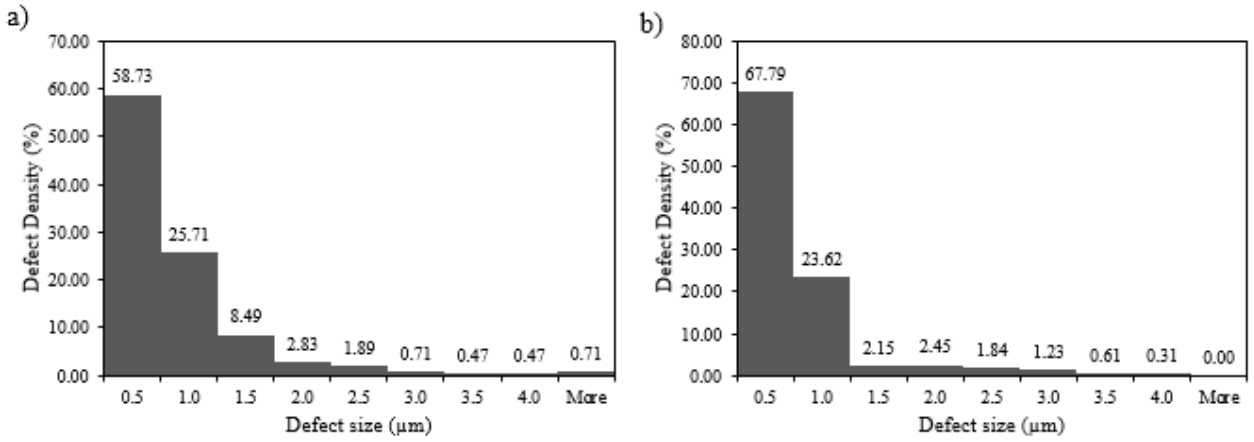

Figure 5. Distribution of the defect size for a) references sample and b) Gap 0.5 samples at the area near the substrate. Higher number of defects with larger size was found for the reference sample compared to the Gap 0.5 sample.

The porous areas formed in the samples at the regions away from the substrate (far from the cubic border for the Gap 0.5 sample) were depicted in figure 6. Similar to the area near the substrate, a smaller number of pores can be found for Gap 0.5 sample (figure 6b) versus the reference sample (figure 4a). However, compared to the region near the substrate, a lower density of pores (0.088% and 0.056% for reference and Gap 0.5 sample, respectively) can be seen for both samples which shows more densification level for the areas away from the substrate. This result was also observed in the previous study by authors [40], where lesser number of defects and higher quality were found for the areas away from the substrate in the as-fabricated LPBF processed samples. Figure 7 shows the size distribution of porosities for both samples at the area away from the substrate. Similar to the region near the substrate, larger pores have higher percentage for the reference sample. Also by comparing the distribution plots between both areas, the proportion of larger pores (bigger than 1.5 µm) is noticeably lower for the region away from the substrate. As mentioned previously, the higher temperature gradient exists between the first layers of the sample and substrate resulting in adequate residual stress [41] to form defects including surface defects and porosities [42]. That is why a higher level of surface porosity was found in the areas near the substrate for both samples, with the border reducing the formation of the pores up to an extent.

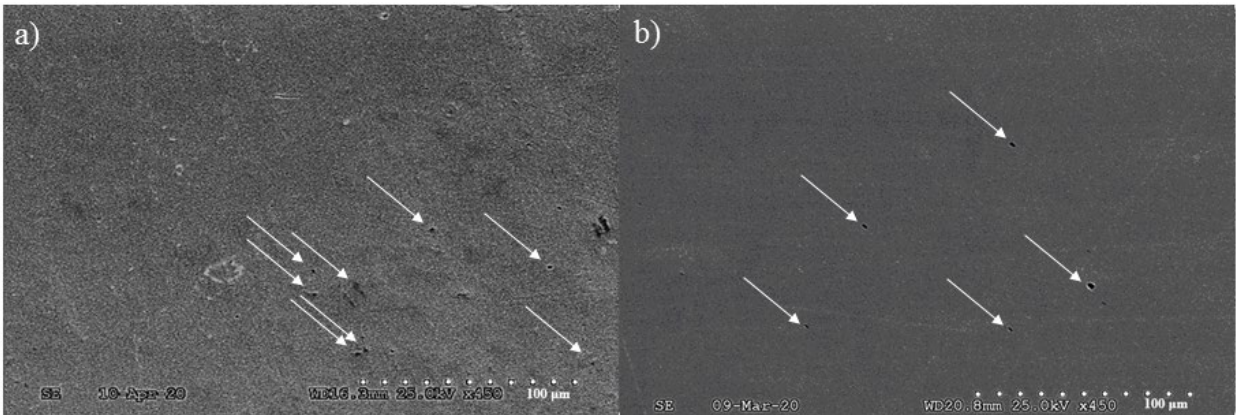

Figure 6. SEM micrographs showing porous areas formed in areas away from the substrate for a) reference sample, b) gap 0.5 sample. More porous areas were found on the reference sample versus Gap 0.5 sample. However, number of porous areas decreased for both samples at the region away from the substrate.

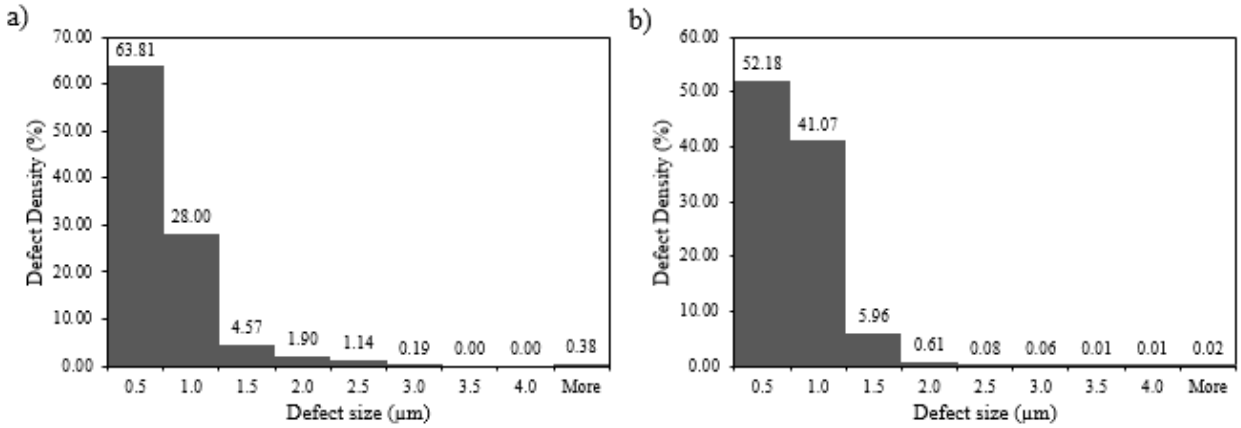

Figure 7. Distribution of the defect size for a) references sample and b) Gap 0.5 samples at the area far from the substrate. While the density of larger defects is lower for the Gap 0.5 sample, the percentage of large-size defects (larger than 1.5 µm) decreased for both samples at the area away from the substrate compared to the region near the substrate.

3.2 Hardness Analysis

Figure 8 showcases the Vickers hardness results for both samples generated at areas near (close to the cubic border for the Gap 0.5 sample) and away the substrate (far from the cubic border for the Gap 0.5 sample). Regradless of the focus area, higher hardness value was found for the Gap 0.5 sample. Generally, it has been reported that the interface condition and the level of bonding between solidified phases can lead to the local variation in hardness value [43-45]. Since more cohesive boundaries between the pools was found for the Gap 0.5 sample compared to the reference sample, higher hardness value was expected for this sample. Also, as more overlap between the melt pools

was observed for the Gap 0.5 sample, more cyclic reheating occurs for this sample. This resembles the heat treatment process which facilitates the dispersion of secondary strengthening particles more evenly in this sample [5, 17, 46] and thereby results in higher hardness values. This phenomenon has been reported for the direct aged samples due to the increase in the level of Nb among subgrains, which facilitates precipitation of secondary (γ″ and γ′) phases and improves the hardness value [47, 48]. A similar process takes place for the Gap 0.5 sample as higher level of melt pool overlapping and thus formation of deeper pools observed for this samples. As a consequence, finer but more evenly distributed strengthening secondary phase (γ″) in the regions surrounded by the border, leading to higher hardness values. However, for both samples, an improvement in hardness value can be observed for the areas away from the substrate versus the regions near the substrate. The value observed for the Gap 0.5 sample (397 HV) is higher than the values reported in literature for IN718 as-built LPBF sample (322 HV) [49], heat treated LPBF sample (335 HV), as-fabricated wrought (151±80) [50] and cast parts (353 HV) [51]. The higher values found for the areas away from the substrate is consistent with the previous study [40], with the highest hardness value being observed for the area close to the center of the sample. It has been revealed that the microhardness value can be improved significantly for a crack and pore free structure [52]. As it was observed for the area away from the substrate, considerably less porous areas were formed compared to the area near the substrate. This explains our results showing higher Vickers hardness value for the area away from the substrate.

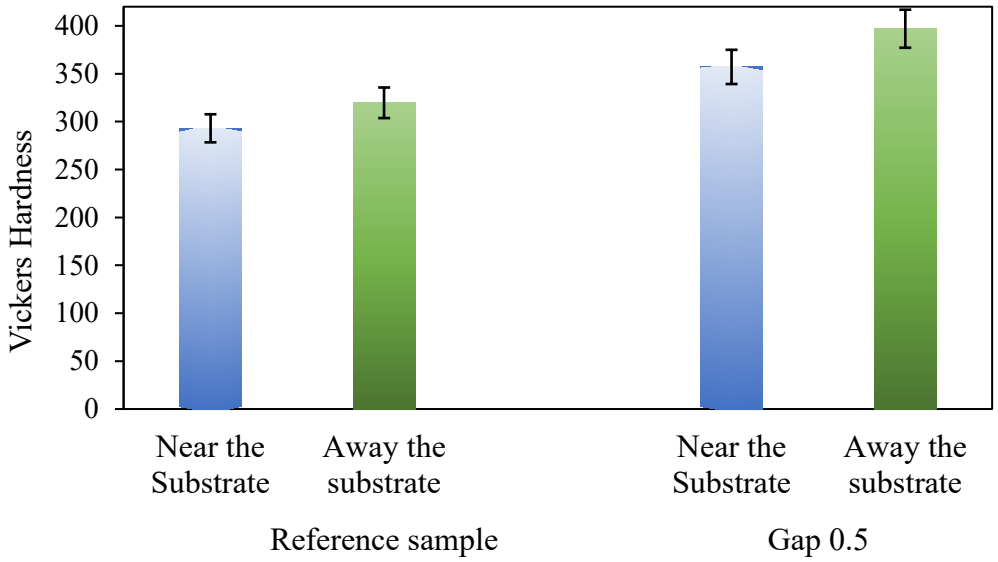

Figure 8. Vickers Hardness values for both samples at the areas near and away the substrate. In both areas, higher hardness value was found for the Gap 0.5 sample compared to the reference sample. A higher hardness was observed for both samples in regions away from the substrate compared to the areas near the substrate.

Based on the comparison of results performed between the areas near and away the substrate, it was observed that using a cubic border surrounding the main sample can lead to better microstructure and properties in LPBF process. However, the level of homogeneity along the build direction did not improve when the border was used. The same variation was observed for both the as-fabricated samples. The authors expect that using a different geometry for the border, in which the gap value between the main sample and border changes gradually along the build direction, may

result in an improvement in the level of homogeneity as well as density, hardness, and mechanical properties. Further studies are required to investigate the effect of using a tapered border on the properties and microstructure homogeneity of the LPBF fabricated samples.

4. Conclusion

In this study, the effect of a surrounding cubic border on the level of homogeneity in properties of LPBF-fabricated parts was investigated. Specifically, the variation of the microstructure and properties along the building direction for the samples fabricated with and without border was examined. The results were compared between the areas near and away the substrate. It was found out that, regardless of the focused area, using a cubic border result in the formation of deeper pools, higher level of density, and higher hardness value for the sample. A variation in the microstructure and properties was observed for both as-fabricated samples (with/without the cubic border). Deeper pools, less surface porosity, and higher Vickers hardness was found in both samples for areas away from the substrate. It was concluded that although surrounding a sample by a cubic border brought about better mechanical and microstructural properties; it failed to improve the homogeneity in properties along the build direction. A parametric study on the border is needed to achieve both homogeneity and better properties in LPBF process.

5. Acknowledgement

This work was supported by a University of Texas System STARs award.

6. References

1. Calandri, M., et al., *Texture and Microstructural Features at Different Length Scales in Inconel 718 Produced by Selective Laser Melting.* Materials, 2019. **12**(8): p. 1293.
2. Beaman, J.J., et al., *Solid Freeform Fabrication: A New Direction in Manufacturing*. Vol. 1. 1997: Springer US. IX, 330.
3. Chua, C.K., K.F. Leong, and C.S. Lim, *Rapid Prototyping, Principles and Applications.* Assembly Automation, 2010. **30**(4).
4. Mostafa, A., et al., *Structure, Texture and Phases in 3D Printed IN718 Alloy Subjected to Homogenization and HIP Treatments.* Metals, 2017. **7**(6).
5. Amato, K.N., et al., *Microstructures and mechanical behavior of Inconel 718 fabricated by selective laser melting.* Acta Materialia, 2012. **60**(5): p. 2229-2239.
6. Thomas, A., et al., *High Temperature Deformation of Inconel 718.* Journal of Materials Processing Technology, 2006. **177**: p. 469-472.
7. Pieraggi, B. and J.-F. Uginet. *Fatigue and creep properties in relation with alloy 718 microstructure* 1998.
8. Holland, S., et al., *Multiscale characterization of microstructures and mechanical properties of Inconel 718 fabricated by selective laser melting.* Journal of Alloys and Compounds, 2019. **784**: p. 182-194.
9. Popovich, V.A., et al. *Creep and Thermomechanical Fatigue of Functionally Graded Inconel 718 Produced by Additive Manufacturing*. 2018. Cham: Springer International Publishing.

10. DebRoy, T., et al., *Additive manufacturing of metallic components – Process, structure and properties.* Progress in Materials Science, 2018. **92**: p. 112-224.
11. Murr, L.E., et al., *Fabrication of Metal and Alloy Components by Additive Manufacturing: Examples of 3D Materials Science.* Journal of Materials Research and Technology, 2012. **1**(1): p. 42-54.
12. Murr, L.E., *Metallurgy of additive manufacturing: Examples from electron beam melting.* Additive Manufacturing, 2015. **5**: p. 40-53.
13. Jia, Q. and D. Gu, *Selective laser melting additive manufacturing of Inconel 718 superalloy parts: Densification, microstructure and properties.* Journal of Alloys and Compounds, 2014. **585**: p. 713-721.
14. Kuo, Y.-L., S. Horikawa, and K. Kakehi, *The effect of interdendritic δ phase on the mechanical properties of Alloy 718 built up by additive manufacturing.* Materials & Design, 2017. **116**: p. 411-418.
15. Gong, X. and K. Chou. *Microstructures of Inconel 718 by Selective Laser Melting*. 2016. Cham: Springer International Publishing.
16. Murr, L.E., et al., *Microstructural Architecture, Microstructures, and Mechanical Properties for a Nickel-Base Superalloy Fabricated by Electron Beam Melting.* Metallurgical and Materials Transactions A, 2011. **42**(11): p. 3491-3508.
17. Wang, Z., et al., *The microstructure and mechanical properties of deposited-IN718 by selective laser melting.* Journal of alloys and compounds, 2012. **513**: p. 518-523.
18. Yan, C., et al., *Evaluations of cellular lattice structures manufactured using selective laser melting.* International Journal of Machine Tools and Manufacture, 2012. **62**: p. 32-38.
19. Gebhardt, A., et al., *Additive Manufacturing by selective laser melting the realizer desktop machine and its application for the dental industry.* Physics Procedia, 2010. **5**: p. 543-549.
20. Qi, H., M. Azer, and A. Ritter, *Studies of Standard Heat Treatment Effects on Microstructure and Mechanical Properties of Laser Net Shape Manufactured INCONEL 718.* Metallurgical and Materials Transactions A, 2009. **40**(10): p. 2410-2422.
21. Maamoun, A.H., et al., *The Effect of Selective Laser Melting Process Parameters on the Microstructure and Mechanical Properties of Al6061 and AlSi10Mg Alloys.* Materials, 2019. **12**(1): p. 12.
22. Gong, X., et al., *Characterization of Microstructure and Mechanical Property of Inconel 718 from Selective Laser Melting*. 2015.
23. Trosch, T., et al., *Microstructure and mechanical properties of selective laser melted Inconel 718 compared to forging and casting.* Materials Letters, 2016. **164**: p. 428-431.
24. Lu, Y., et al., *Study on the microstructure, mechanical property and residual stress of SLM Inconel-718 alloy manufactured by differing island scanning strategy.* Optics & Laser Technology, 2015. **75**: p. 197-206.
25. Ravichander, B.B., et al., *A Prediction Model for Additive Manufacturing of Inconel 718 Superalloy.* Applied Sciences, 2021. **11**(17).
26. Moussaoui, K., et al., *Effects of Selective Laser Melting additive manufacturing parameters of Inconel 718 on porosity, microstructure and mechanical properties.* Materials Science and Engineering: A, 2018. **735**: p. 182-190.
27. Nadammal, N., et al., *Effect of hatch length on the development of microstructure, texture and residual stresses in selective laser melted superalloy Inconel 718.* Materials & Design, 2017. **134**: p. 139-150.

28. Choi, J.-P., et al., *Densification and microstructural investigation of Inconel 718 parts fabricated by selective laser melting.* Powder Technology, 2017. **310**: p. 60-66.
29. Popovich, A.A., et al., *Design and manufacturing of tailored microstructure with selective laser melting.* Materials Physics and Mechanics, 2018. **38**: p. 1-10.
30. Ravichander, B.B., A. Amerinatanzi, and N. Shayesteh Moghaddam, *Study on the Effect of Powder-Bed Fusion Process Parameters on the Quality of as-Built IN718 Parts Using Response Surface Methodology.* Metals, 2020. **10**(9).
31. Kumar, P., et al., *Influence of laser processing parameters on porosity in Inconel 718 during additive manufacturing.* The International Journal of Advanced Manufacturing Technology, 2019. **103**(1): p. 1497-1507.
32. Wang, X. and K. Chou, *Microstructure simulations of Inconel 718 during selective laser melting using a phase field model.* The International Journal of Advanced Manufacturing Technology, 2019. **100**(9): p. 2147-2162.
33. Zhang, D., et al., *Thermofluid field of molten pool and its effects during selective laser melting (SLM) of Inconel 718 alloy.* Additive Manufacturing, 2018. **21**: p. 567-578.
34. Ravichander, B.B., et al., *Analysis of the deviation in properties of selective laser melted samples fabricated by varying process parameters*. SPIE Smart Structures + Nondestructive Evaluation. Vol. 11377. 2020: SPIE.
35. Vander Voort, G. and E. Manilova, *Metallographic Techniques for Superalloys.* Microscopy and Microanalysis, 2004. **10**(S02): p. 690-691.
36. ImageJ, R.W., *ImageJ, R.W., US Natl Institutes Heal Bethesda, Maryland, USA. 2012.* .
37. NASA, *Specification for Control and Qualification of Laser Powder Bed Fusion Metallurgical Processes*. 2017: Marshall Space Flight Center, Alabama.
38. Kruth, J.-P., et al., *Part and Material Properties in Selective Laser Melting of Metals*, in *Proceedings of the 16th International Symposium on Electromachining (ISEM XVI)*. 2010. p. 3-14.
39. Jokisch, T., et al., *Laser Welding of SLM-Manufactured Tubes Made of IN625 and IN718.* Materials, 2019. **12**(18): p. 2967.
40. Farhang, B., et al., *Study on variations of microstructure and metallurgical properties in various heat-affected zones of SLM fabricated Nickel–Titanium alloy.* Materials Science and Engineering: A, 2020. **774**: p. 138919.
41. Mercelis, P. and J.P. Kruth, *Residual stresses in selective laser sintering and selective laser melting.* Rapid Prototyping Journal, 2006. **12**(5): p. 254-265.
42. Parry, L.A., I.A. Ashcroft, and R.D. Wildman, *Geometrical effects on residual stress in selective laser melting.* Additive Manufacturing, 2019. **25**: p. 166-175.
43. Soffel, F., et al., *Interface strength and mechanical properties of Inconel 718 processed sequentially by casting, milling, and direct metal deposition.* Journal of Materials Processing Technology, 2021. **291**: p. 117021.
44. Osmanson, A.T., et al. *Mechanisms of Contact Formation and Electromigration Reliability in Wirebond Packages*. in *2021 IEEE International Reliability Physics Symposium (IRPS)*. 2021.
45. Tajedini, M., et al. *Electromigration Effect on the Pd Coated Cu Wirebond*. in *2021 IEEE 71st Electronic Components and Technology Conference (ECTC)*. 2021.
46. Zhang, D., et al., *Effect of standard heat treatment on the microstructure and mechanical properties of selective laser melting manufactured Inconel 718 superalloy.* Materials Science and Engineering: A, 2015. **644**: p. 32-40.

47. Tucho, W.M. and V. Hansen, *Studies of Post-Fabrication Heat Treatment of L-PBF-Inconel 718: Effects of Hold Time on Microstructure, Annealing Twins, and Hardness.* Metals, 2021. **11**(2): p. 266.
48. Jiang, R., et al., *Varied heat treatments and properties of laser powder bed printed Inconel 718.* Materials Science and Engineering: A, 2019. **755**: p. 170-180.
49. Parimi, L.L., et al., *Microstructural and texture development in direct laser fabricated IN718.* Materials Characterization, 2014. **89**: p. 102-111.
50. Muhammad, M., et al., *An investigation into the effects of cyclic strain rate on the high cycle and very high cycle fatigue behaviors of wrought and additively manufactured Inconel 718.* International Journal of Fatigue, 2021. **144**: p. 106038.
51. Popovich, V.A., et al., *Impact of heat treatment on mechanical behaviour of Inconel 718 processed with tailored microstructure by selective laser melting.* Materials & Design, 2017. **131**: p. 12-22.
52. Elahinia, M., et al., *Fabrication of NiTi through additive manufacturing: A review.* Progress in Materials Science, 2016. **83**: p. 630-663.